Accumulation of styrene oligomers alters lipid membrane phase order and miscibility

Mattia Morandi, Monika Kluzek, Jean Wolff, André Pierre Schroder, Fabrice Thalmann, Carlos Marques

Accumulation of styrene oligomers alters lipid membrane phase order and miscibility

Mattia I. Morandi[a,1], **Monika Kluzek**[a], **Jean Wolff**[a], **André Schroder**[a], **Fabrice Thalmann**[a], **and Carlos M. Marques**[a,1]

[a]Université de Strasbourg, CNRS, Institut Charles Sadron, UPR022, 23 rue du Loess, 67034 Strasbourg Cedex, France

This manuscript was compiled on October 17, 2020

Growth of plastic waste in the natural environment, and in particular in the oceans, has raised the accumulation of polystyrene and other polymeric species in eukyarotic cells to the level of a credible and systemic threat. Oligomers, the smallest products of polymer degradation or incomplete polymerization reactions, are the first species to leach out of macroscopic or nanoscopic plastic materials. However, the fundamental mechanisms of interaction between oligomers and polymers with the different cell components are yet to be elucidated. Simulations performed on lipid bilayers showed changes in membrane mechanical properties induced by polystyrene, but experimental results performed on cells membranes or on cell membrane models are still missing. We focus here on understanding how embedded styrene oligomers affect the phase behavior of model membranes using a combination of scattering, fluorescence and calorimetric techniques. Our results show that styrene oligomers disrupt the phase behavior of lipid membranes, modifying the thermodynamics of the transition through a spatial modulation of lipid composition.

Nanopollution | Lipid bilayer phase separation | SANS | LAURDAN

The increasing amount of plastic present in sea waters has become a major issue in recent years, with raising concerns regarding the potential hazardous effects it may have on living systems (1, 2). Annual production of plastic has reached almost 300 million tons per year, of which 5 to 13 million tons are estimated to reach the oceans by different means (3). While initially the main concern for plastic contamination was the presence of microplastic, produced by polymeric degradation, recently the focus has shifted to nanoplastic (4, 5). Objects of this scale can easily enter the food chain via digestion and there is increasing evidence of plastic micro and nano-objects found in the marine life forms (6–9). Moreover, nanometer-size polymer particles are also produced industrially for specific research and technological applications, such as imaging, sensing, and preparation of nanocomposites (10), providing a second route, besides degradation, for plastic-derived nanoparticles entry into sea waters. Despite a current lack of evidence on the presence of nanoobjects (4), studies have indeed shown that plastic nanoparticles can accumulate in the tissues of living organisms and disrupt their metabolism (11–13), and that size plays an important role in determining their accumulation (12, 13). However, a physicochemical characterization of the interaction between plastic nanoobjects and living organisms is still lacking, especially regarding the mechanisms of potential toxicity. As the first barrier encountered by any foreign object entering an organism, the cell membrane is the primary candidate of investigation in assessing possible toxicity of plastic nano fragments. In particular, the membrane lipid lateral organization plays a crucial role in many cellular signalling processes due to the presence in the membrane of small transient domains called "lipid rafts", and even minute changes in membrane lipid organization can result in a potential alteration of these processes and pose a threat to cellular viability.

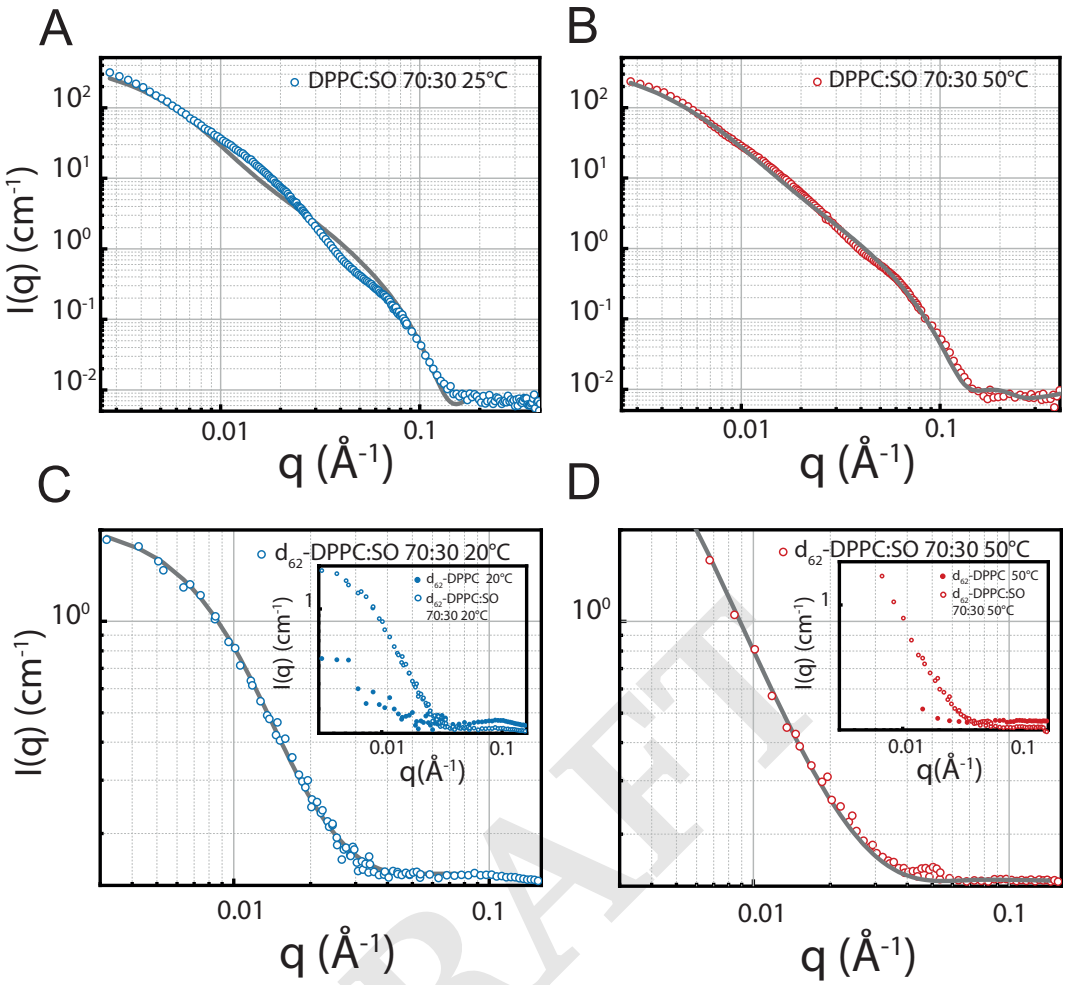

Fig. 1. SANS scattering curves for 50 nm SUVs and relative fittings. (A) Fitting with a bilayer model of DPPC:SO scattering curves at 25°C. (B) Fitting with a bilayer model of DPPC:SO scattering curves at 50°C. (C) Fitting of SANS scattering curves for d_{62}-DPPC:SO 70:30 at 20°C. Inset shows comparison of scattering signal between d_{62}-DPPC and d_{62}-DPPC:SO liposomes at 20°C (D) Comparison of d_{62}-DPPC and d_{62}-DPPC:SO liposomes at 50°C. Inset shows comparison of scattering signal between d_{62}-DPPC and d_{62}-DPPC:SO liposomes at 50°C. All plots are represented as experimental data (circles) and relative fitting (grey line). Both fittings for (C) and (D) were performed using Sasfit implemented thin disk model. The signal arising from the pure lipid samples displays very low intensity due to the matching of scattering density between solvent and lipids. In case of 20°C, the signal appears slightly more intense due to changes in the scattering lenght density of lipids.

Polystyrene is one of the most commonly used plastic in the world, contributing to a significant fraction of marine plastic wastes in the form of styrene oligomers (SO) (14), and it has been shown in several studies to directly affect lipid bilayer physical properties when accumulated within the membrane. Accumulation of styrene oligomers and polymers in POPC bilayers indeed showed, in numerical simulations, to change the membrane mechanical properties and lateral lipid organization (15), and a stabilization of cholesterol induced domains (16). However, experimental studies on the effects of polystyrene and oligomers

Significance Statement

Accumulation of nanopollutants in lifeforms has become the subject of increasing concern, but effects are not understood. Biological systems are inherently complex, therefore any small variations on the membrane properties can potentially perturb cell functionality. In this study we observe that the presence of styrene oligomers in lipid membranes alters their phase behavior, with stronger changes occurring in more complex systems, which could translate in potential cellular disruption. This study provides evidence that presence of nanopollutants in the membrane may alter its fundamental properties and affect cell viability.

M.I.M. designed the project, executed the calorimetry, fluorescence and microscopy measurements, and wrote the manuscript. M.K. designed the SANS experimental approach, acquired the scattering data and provided the model fitting. J.W. developed the theoretical model for phase separation and contributed to the theoretical fitting. A.S. supervised the fluorescence and microscopy experiments and revised the manuscript. F.T. designed and supervised the project, developed the theoretical model and wrote the manuscript. C.M.M. designed and supervised the project, developed the theoretical model and contributed to the theoretical fitting, and wrote the manuscript. All authors revised the manuscript.

The authors declare no conflict of interest.

[1]To whom correspondence should be addressed. E-mail: marques@unistra.fr, mattia.morandi@weizmann.ac.il

in cell membrane and model membranes are still lacking. It was previously reported that incorporation of styrene monomers into lipid membranes significantly changes the fluidity of the membrane (17), and a similar effect was indeed shown for charged polystyrene sulfonated chains in surfactant bilayers (18), but from an experimental point of view many aspects of the interaction are still elusive. In this work we investigate the effects of styrene oligomers (M_n = 500 Da) on the phase transition of lipids bilayers composed of unsaturated lipids or a mixture of unsaturated/saturated lipids, in order to obtain a more comprehensive picture of the role of membrane complexity on the effects of styrene oligomers accumulation. We investigated the changes in transition using differential scanning calorimetry (DSC), small angle neutron scattering (SANS) and and Laurdan fluorescence spectra to extract information on the structure and the thermodynamics. Moreover, we directly visualized the changes on the membranes at the micrometric scale using epifluorescence microscopy.

Results

Our experimental results focus on two main aspects of styrene oligomers-lipid interaction: first we employed small angle neutron scattering (SANS) both to confirm the presence of the oligomers within the lipid membrane and to obtain information about the changes on the bilayer structure they induce. Subsequently, we focused on changes in the thermodynamics properties and phase behavior of the membrane caused by inclusion of these short styrene chains.

Fluid and gel phases of DPPC lipid membranes can host a high amount of styrene oligomers. For SANS, we utilized liposomes formed either of DPPC in D_2O as a solvent, to maximize scattering contrast, or d_{62}-DPPC (DPPC lipids with all the hydrogen molecules in the carbon chains replaced by deuterium) vesicles in H_2O/D_2O mixture to mask the signal from the lipids and maximize polymer signal. In both lipidic compositions we compared changes between lipid-only liposomes and liposomes formed with 30% mol of styrene oligomers, and scattering curves were acquired at both 20°C and 50°C to investigate the differences between gel and fluid phase. Herein we will report a brief description of the results, a more comprehensive analysis of the SANS data can be found in *SI Appendix*. Fig. 1 shows the scattering curves of DPPC:SO 70:30 and d_{62}-DPPC:SO 70:30 with their respective model fitting. In case of DPPC:SO (Fig. 1 A and B), we observe a good agreement between our data and a bilayer model, particularly for scattering curves at 50°C (Fig. 1 B). Contrarywise, for DPPC:SO at 25°C the fitting strongly deviates from the scattering curve in the intermediate region, indicating a membrane structural change occurring in the gel phase due to the presence of SO. A similar feature has been reported before by Pencer *et al.* (19) for membranes displaying liquid domains coexistence, and they suggested that changes in the scattering curve in that region might be linked to membrane lateral segregation and heterogeneities in scattering length density. The fitting deviates in the intermediate q region. The good values of model fitting for DPPC:SO system suggest that upon incorporation of oligomers we still maintain a liposomal suspension with no additional structures, such as aggregates or micelles. This result was also confirmed via DLS, where we observe one single peak in the size distribution of the liposomes (Fig. SI 6). Scattering curves for d_{62}-DPPC vesicles further confirm the presence of styrene oligomers within the membrane. Fig. 1 C and D show the data obtained when the lipid signal is masked. The clear increase in scattering intensity in systems containing SO compared to d_{62}-DPPC only vesicles (insets of Fig. 1 C and D) is due to the presence of oligomers in the membrane.

Phase changes of the lipid bilayer result in styrene oligomers re-organization. To better understand the oligomer distribution within the lipid bilayer both in the gel (S_o) and fluid (L_α) phases, we extrapolated the structural data for the bilayer under lipid-masking conditions in presence of styrene oligomers. Fitting of the experimental curves was performed using a disk model, motivated by previous analyses of phase separation in model membranes using SANS, where domains were fitted using a similar form factor (20), and obtained good agreement with the data (Fig. 1 C and D). We observe that in the gel phase polystyrene appears to aggregate with an average diameter of 349 ± 0.3 Å, smaller than the liposome size, and with a thickness of 38.3 ± 0.1 Å, comparable to the hydrophobic region of the bilayer. The fitting values are compatible with an heterogenous lateral distribution of the polymer, as it was hinted by the strong deviation from a bilayer scattering in DPPC:SO in D_2O (Fig. 1 A). Moreover, the resulting thickness is comparable with the values obtained for DPPC using a model-free approach (Kratky-Porod and Modified Kratky-Porod at 25°C (Figs. SI 3 and SI 4). In case of the polymer distribution in the fluid phase, we argue that the lack of a visible inflection point in the scattering curve for 50°C reflects a change in lateral distribution of the polymer, which becomes more homogeneously dispersed within the bilayer, and not a real change in diameter of the vesicles. However, since it was not possible to verify the values for the diameter of the disc, we took into consideration only the value for the thickness, which resulted to be 34.0 ± 0.1 Å. This is once again comparable with the bilayer thickness obtained for DPPC:SO liposomes (Table SI 1), hinting that both in gel and fluid phase the polymer is intercalated in the acyl chains.

Vesicle containing SO have higher membrane order. The Laurdan emission spectra for DPPC liposomal suspensions containing increasing molar fractions of SO (sl SI Appendix, Fig. S7), and the calculated corresponding general polarization (GP) values for each temperature probed (Fig. 2 A), highlight changes in the membrane order upon incorporation of the oligomers. The GP values obtained for pure DPPC liposomes in the gel and fluid phase are consistent with previously reported GP curves for DPPC (21), with a GP in the gel phase remaining almost constant at 0.50 ± 0.01, and with a sharp decrease after T_m, to a negative value of -0.33 ± 0.01 at 60°C. Incorporation of the polymer in the membrane does not significantly induce any variation at low temperatures, with a slight increase to 0.54 ± 0.01 for 30% molar fraction of styrene oligomers being observed. In contrast, presence of the polymer strongly shifts the GP to more positive values in the fluid phase, up to -0.13 ± 0.01 for the maximal polymer fraction investigated. We observe a clear dependence of the GP variation on the polymer content (Fig. 2

A inset), that we here argue is due to a uniform distribution of the oligomers within the membrane. The difference in variation of GP, minimal in the gel phase and maximal for the liquid crystalline phase, indicates a different behavior of the polymer between the S_o and L_α. Laurdan spectral properties in different phases of the bilayer have been directly linked to the hydration in the glycerol backbone region of the lipids and to the degree of tail alignment (22). Therefore the increase in GP suggests a lower number of water molecules in the fluid phase of the bilayer due to the presence of polystyrene, hinting also at a higher packing order of the lipids induced by SO. Such an effect might be indicative of intercalation of styrene oligomers through the lipid chains in the fluid phase. A similar effect was reported for incorporation of hydrophobic monoterpenes, where an increase of the order parameter of the acyl chains, particularly the carbon groups closer to the interface (23). In the case of styrene oligomers, the lack of a hydrophilic headgroup prevents the polymer from being exposed to the water-acyl chain interface, however the observed shift in GP, indicative of a higher order of the chain closer to the headgroup region, suggest that at least a significant portion of the oligomers is not confined in the mid plane of the hydrophobic region. This picture is consistent with neutron scattering results reported by Richter *et al.* (24) in case of styrene monomers interacting with DMPC vesicle, where the distribution of the monomers was found to be a coexistence of molecules highly segregated in the midplane and molecules aligned with the hydrocarbon tails.

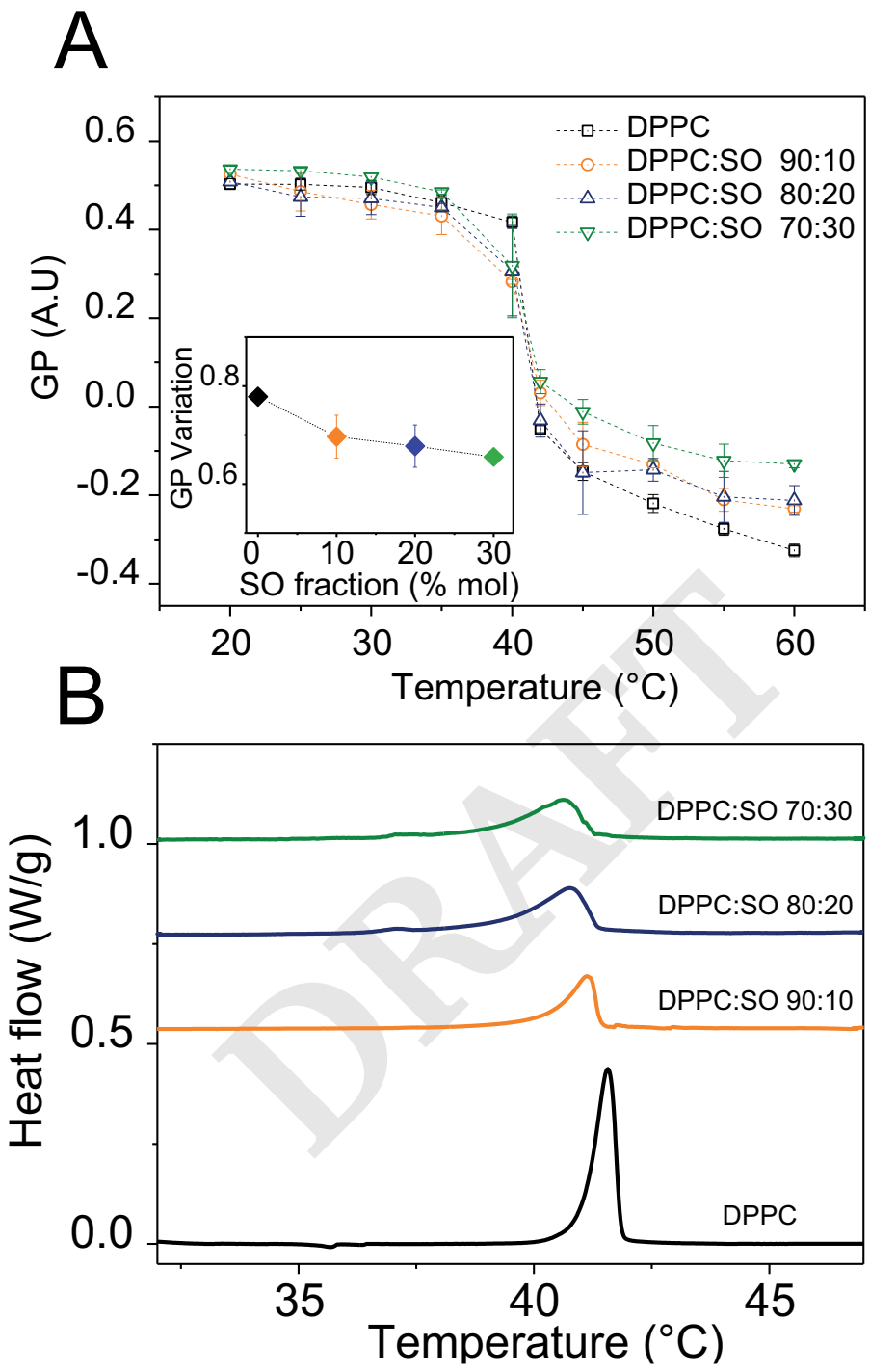

Fig. 2. (A) General polarization (GP) curves over temperature for LUVs of DPPC formed in water at 0% (black squares), 10% (orange circles), 20% (blue triangles) and 30% (green inverted triangles) molar fraction of styrene oligomers. Inset shows the variation of GP between fluid and gel phase for each SO molar fraction, calculated as ΔGP = GP[50°C] - GP[20°C]. Liposomes were extruded to a size of 100 nm. Each data point and error bars represent the average and standard deviation from three (n = 3) separate sample, with 4 technical repeats each. (B) DSC thermographs of DPPC MLVs containing increasing amount of styrene oligomers. Each curve represents the second thermographic signal from the full run experiment. Thermographs provide a determination of the melting temperature T_m (maximum), enthalpy of melting ΔH (area comprised between the baseline and the peak) and transition width $T_{1/2}$ (half height width).

Gel-to-fluid transition is inhibited by PS oligomers. We employed differential scanning calorimetry to measure the gel-to-fluid transition, specifically changes in the enthalpy and transition temperature which could hint at effects on the membrane induced by styrene oligomers. DSC thermographs (Fig. 2 B) show for DPPC-only bilayers a sharp transition peak centered at 41.8 $\pm$ 0.2 °C, in good agreement with data from literature (25). With increasing amount of styrene oligomers incorporated the transition temperature slightly decreases, to a final value of 40.8 $\pm$ 0.4 °C for 30% polymer molar fraction. The peak also significantly decreases in intensity and broadens, suggesting a loss in enthalpy and cooperativity. Calculations of ΔH of the transition yields

a value of 38.5 ± 0.6 kJ· mol^{-1} for pure DPPC, consistent with previously reported data (25). Incorporation of polymer within the bilayer results in a decrease of enthalpy and cooperativity with increase of styrene oligomers amount, as shown in Table 1 and Fig. S8. In particular we observe a linear decrease of ΔH and increase of $T_{1/2}$ with respect to polymer content, whereas T_m does not vary significantly (Fig. SI 9). Our results differ significantly from the previously reported trend for DODAB vesicles incorporating 60% molar fraction of styrene monomers, where a strong decrease in transition temperature and only slight variation of enthalpic contribution was observed (17). However, the effects we observe of decrease in T_m and broadening of the transition peak are in agreement with previously reported studies of incorporation of hydrophobic molecules in lipid bilayers (26, 27). The overall trend of depression of the melting temperature and broadening of the transition are consistent

Table 1. Calculated ΔH, T_m and $T_{1/2}$ for DPPC with increasing molar fractions of styrene oligomers. Values are presented as average and standard deviation from two (n = 2) separate samples, with 6 technical repeats each.

styrene oligomers fraction % mol	ΔH kJ· mol^{-1}	T_m °C	$T_{1/2}$ °C
0	38.5 ± 0.7	41.8 ± 0.2	0.27 ± 0.01
10	30.7 ± 3.8	41.5 ± 0.4	0.29 ± 0.01
20	27.9 ± 1.1	41.2 ± 0.3	0.45 ± 0.01
30	25.1 ± 0.9	40.8 ± 0.4	0.66 ± 0.01

with the effects reported for hydrophobe/lipid bilayer interactions. Wolka *et al.* (28) and Rolland *et al.* (26) reported that incorporation of penetration enhancers reduce the transition temperature of DPPC to 40°C at 10% molar fraction of molecule, as well as a significant increase in the width of the transition peak. Similar results have been found for membranes containing flavonoids, with increasing hydrophobicity of the molecule producing a stronger effect (29, 30). Borsacchio *et al.* also reported similar behavior for incorporation of pheromones in DOPC bilayers (31).

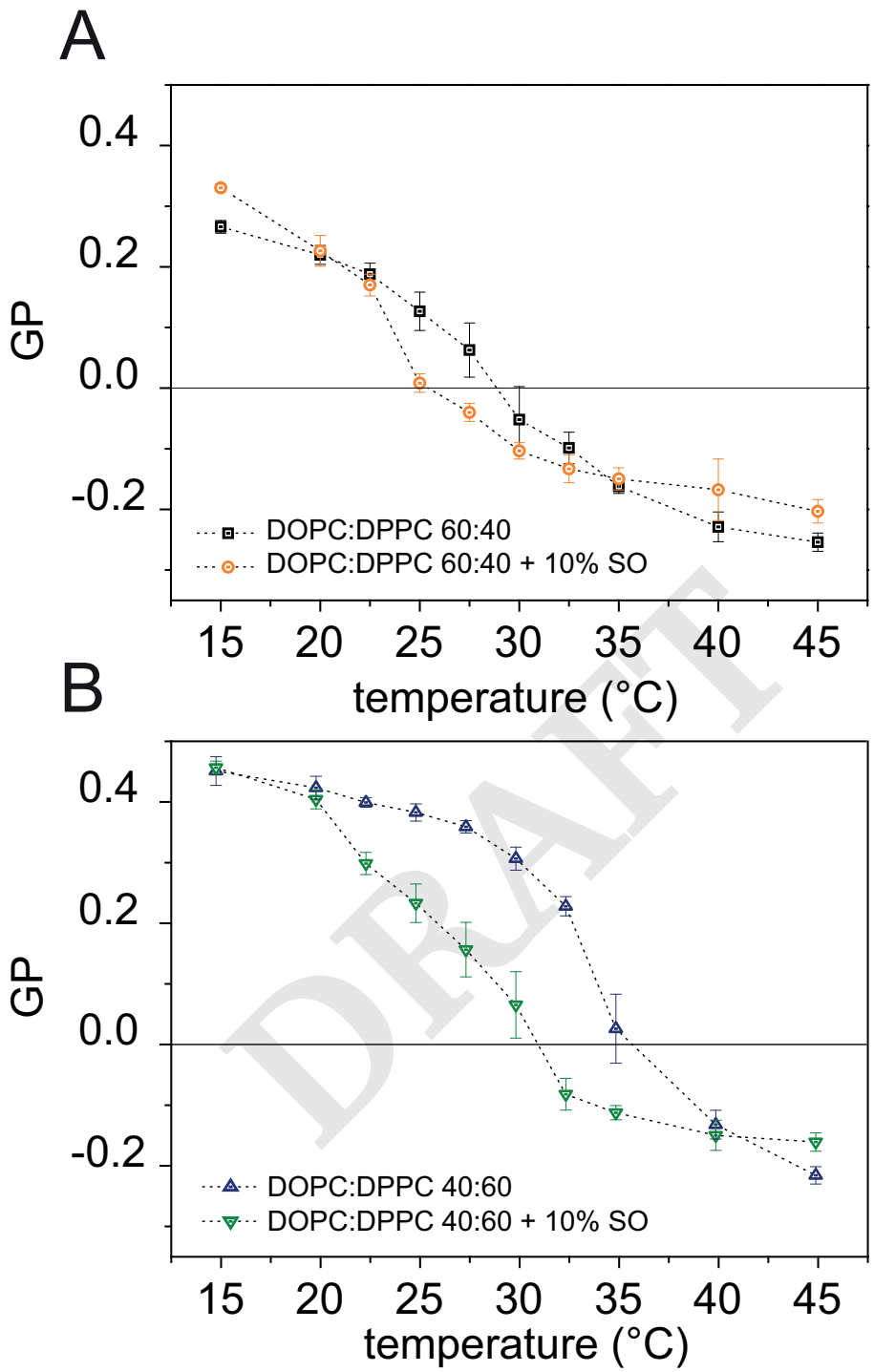

Fig. 3. (A) Variation of General Polarization over temperature for LUVs of DOPC:DPPC 60:40 (black squares) and DOPC:DPPC 60:40 + 10 mol% SO (orange circles). (B) Variation of general polarization over temperature for LUVs of DOPC:DPPC 40:60 (blue triangles) and DOPC:DPPC:SO 40:60 + 10 mol% SO (green inverted triangles).Liposomes were extruded to a size of 100 nm. Each data point and error bars represent the average and standard deviation from three (n = 3) separate sample, with 4 technical repeats each.

Styrene oligomers increase miscibility between S_o and L_α phases. To better understand the effects induced by the styrene oligomers on the phase behavior of lipid bilayers, we probed changes in the Laurdan spectra in liposomes composed of DOPC and DPPC at different compositions (Fig. S9). Calculation of general polarization yield GP curves illustrated in Fig. 3. For

pure DOPC:DPPC liposomes we observe a broad transition, starting from a value of 0.27 ± 0.01 and 0.45 ± 0.01 at 15°C to -0.25 ± 0.02 and -0.21 ± 0.01 at 45°C for DPPC molar fractions of 0.4 and 0.6, respectively. The values at low temperature are much lower than the GP of pure DPPC bilayer (21), indicating a gel/fluid phase coexistence. The miscibility temperature T_m, measured from the intersection of GP curves obtained from excitation wavelengths 350 nm and 400 nm (see Fig. S10), is approximately 28.3 ± 1.5 °C for $X_{\mathrm{DPPC}} = 0.4$ and 34.9 ± 0.9 °C for $X_{\mathrm{DPPC}} = 0.6$, consistently with known values of miscibility for this system (32–36). The values of GP and curve broadness are in agreement with a membrane displaying L_d/S_o coexistence at low temperature and a homogeneous liquid disordered phase above T_m. In the case of systems with the same lipid ratio and additional incorporation of styrene oligomers, we observe significant changes in the Laurdan GP values. For 0.4 DPPC molar fraction the initial value is highly increased to 0.33 ± 0.01 at 15°C, as well as the value in the liquid crystalline phase displays higher GP, with value of 0.22 ± 0.02 at 45°C. Moreover, the transition temperature decreases to 23.4 ± 0.8 °C and the curve becomes sharper. Increasing fraction of DPPC in the membrane seems to slightly reduce this effects, as for $X_{\mathrm{DPPC}} = 0.6$ the initial values of GP are comparable, while at 45°C we observe a slight increase to -0.16 ± 0.02.

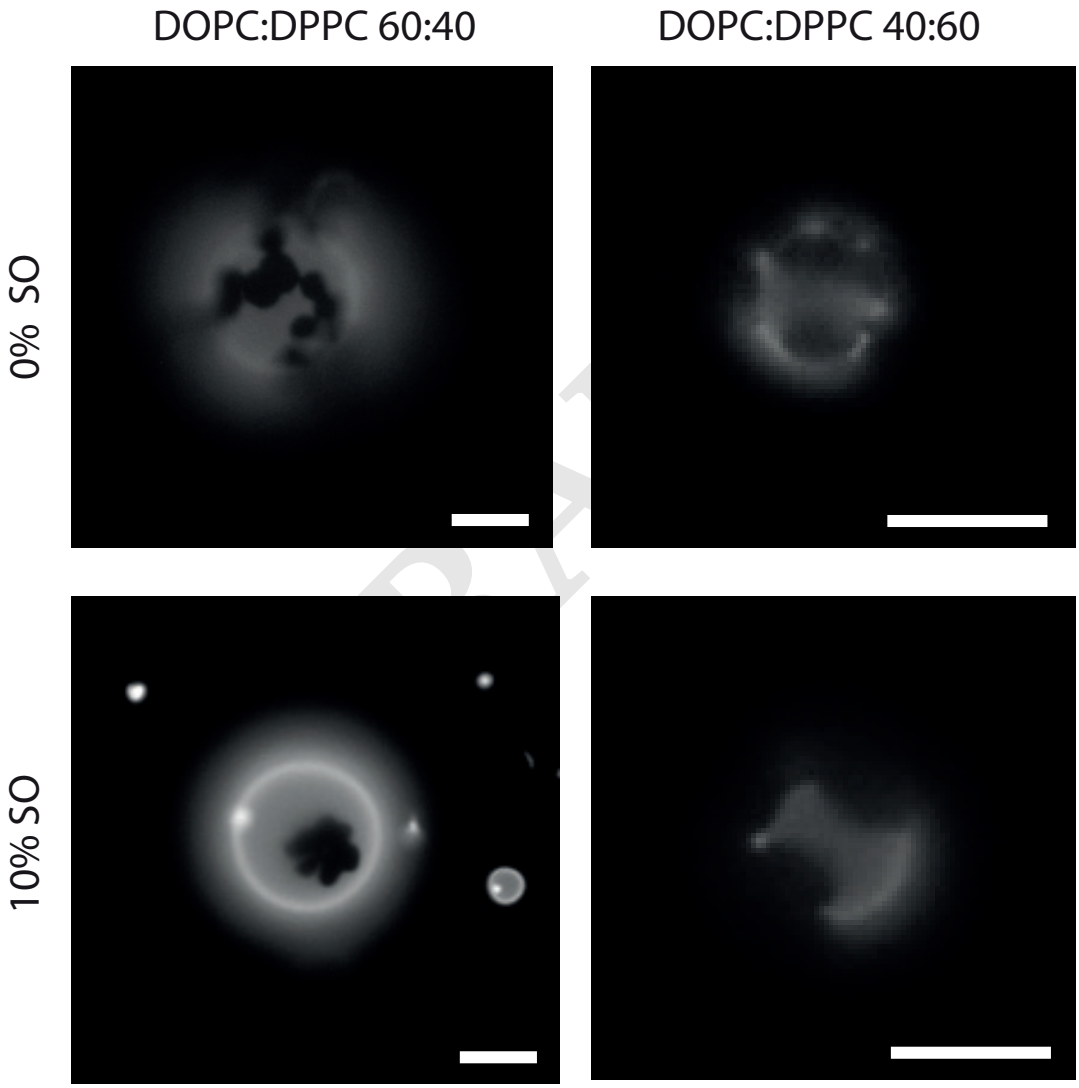

Fig. 4. Representative images of DOPC:DPPC GUVs labelled with 1% mol DiI, without and with 10% mol fraction of SO incorporated, visualized using epifluorescence microscopy. The bright area represents presence of fluorophore, which partitions in the L_α phase. Dark spots are S_o domains. Scale bar 5 μm.

We further confirmed the lowering of the liquidus line observed in the GP plots upon addition of 10% mol SO, by analyzing under epifluorescence microscopy the area coverage of gel phase domains in GUVs composed of different ratios of DOPC and DPPC. Giant unilamellar vesicles at both DOPC:DPPC compositions display fluid/gel coexistence at room temperature, with characteristic S_o domains of irregular or hexagonal morphology (Fig. 4), consistent with previous reported studies (35). For each vesicle we calculated first the area fraction of S_o domains, f_b, in the pure lipid case, and obtained a total area coverage of 0.17 ± 0.03 and 0.47 ± 0.03 for DPPC molar fraction of 0.4 and 0.6, respectively. It is possible to compare measured values for area coverage with theoretically predicted fractions of gel phase by means of the lever rule, benefiting from the almost vertical shape of the solidus line in this region of the phase diagram (32). Assuming thus a constant solidus line at 0.95 for

the considered DPPC molar fraction interval, our values are consistent with theoretical predictions (Table 2), as well as with previously reported coverage of DPPC gel domains in DOPC membranes (35). Since the S_o fraction in GUVs agrees with DOPC:DPPC phase diagrams, we can now measure the gel phase coverage upon addition of 10 mol% of styrene oligomers, while maintaining the same DOPC:DPPC composition. This overall allows to obtain an experimental phase diagram by combining the values obtained by Laurdan and GUVs. Vesicles incorporating 10% mol SO still exhibit S_o/L_α coexistence, with intact domain morphology (Fig. 4); however the solid domain fraction, f_b^{SO}, is greatly reduced. Analysis of the domain coverage yielded a fraction for the solid phase of 0.077 $\pm$ 0.021 and 0.28 $\pm$ 0.06 for 60:40 and 40:60 mixtures, respectively. The values of solid area fraction obtained with GUVs containing SO allow to estimate the liquidus line in presence of 10% mol oligomers. For that reason, we have visualized GUVs containing styrene oligomers at two separate temperatures, namely 20°C and 23°C. Using a solidus line value for each temperature based on previously reported data by Schmidt et al. (32), and using the lever rule, we obtained values for X_a^{SO} of 0.35 $\pm$ 0.05 for 20°C and 0.38 $\pm$ 0.06 for 23°C. We observe that the miscibility temperature obtained both from Laurdan spectra and GUVs confirm the lowering of the liquidus line between S_o-L_α coexistence and pure L_α phase (Fig. 5).

DPPC molar fraction	Experimental S_o fraction (f_b)	Theoretical fraction pure DPPC	Theoretical fraction 0.95 DPPC	S_o fraction w 10% SO (f_b^{SO})
0.4	0.17 $\pm$ 0.03	0.18 $\pm$ 0.01	0.20 $\pm$ 0.01	0.08 $\pm$ 0.02
0.6	0.47 $\pm$ 0.03	0.42 $\pm$ 0.01	0.47 $\pm$ 0.01	0.28 $\pm$ 0.06

Table 2. Summary of S_o area coverage for DOPC:DPPC GUVs at different composition. Each value represents average and standard deviation of two separate samples of 40 vesicles each.

A theoretical model explains the changes in DOPC:DPPC miscibility. Furthermore, we compared our experimental results with a thermodynamics model for binary phase diagrams developed by Wolff *et al.* (36), which considers the gel-to-liquid transition in the framework of mean-field Ising (2 states) model. Simply, for a binary lipid mixture the thermodynamics of the gel-to-liquid transition of a binary mixtures can be written as:

$$\begin{aligned}\mathcal{G}^{\text{mix}}(T,\phi_1,\phi_2,m) = &-m[h_1(T)\phi_1 + h_2(T)\phi_2] - 2Jm^2 \\ &+ (\frac{1+m}{2})\ln(\frac{1+m}{2}) + (\frac{1-m}{2})\ln(\frac{1-m}{2}) \\ &+ \phi_1\ln(\phi_1) + \phi_2\ln(\phi_2)\end{aligned} \quad [1]$$

with

$$h_1(T) = \frac{\Delta H_1}{2RT_1^2}(T - T_1),\ h_2(T) = \frac{\Delta H_2}{2RT_2^2}(T - T_2) \quad [2]$$

where ϕ_1 and ϕ_2 are the area fractions of the two lipid species, J is the mismatch energy associated with the interaction between two neighbouring lipids, m is a non-conserved scalar order parameter restricted to the interval $[-1, 1]$, R is the gas constant, ΔH_1 and ΔH_2 are the respective gel-to-liquid enthalpies of melting and T_1 and T_2 the respective transition temperatures. Changes in area per lipid at the transition are not taken into account. The thermodynamic potential $\mathcal{G}^{\text{mix}}$ represents the ratio $G/\mathcal{A}_l RT$ of the Gibbs free-energy of mixing of the hydrated lipid bilayer divided by the total area of lipids $\mathcal{A}_l$ and temperature T, while m interpolates continuously between negative (gel state) and positive (fluid state) values. Phase coexistence results from minimization of $\mathcal{G}^{\text{mix}}$ with respect to m followed by convex minimization with respect to ϕ_1 and ϕ_2.

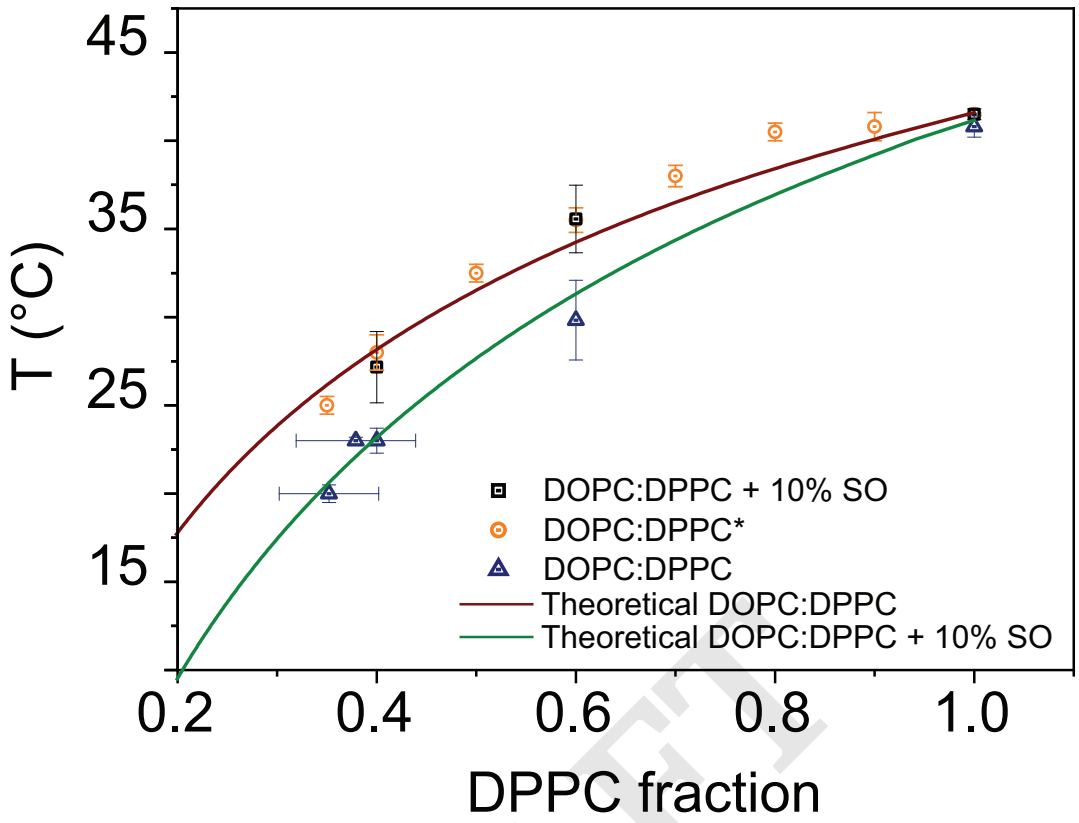

Fig. 5. Comparison between experimental data point for the liquidus line estimated by results from Chen *et al.* (35) (orange), experimental data point for DOPC:DPPC (blue triangles) and DOPC:DPPC:SO (black squares) obtained from Laurdan emission spectra, and theoretical predictions of liquidus lines for DOPC:DPPC (red) and DOPC:DPPC + 10%SO (green).

For DOPC:DPPC bilayers we calculated the phase diagram using values of $\Delta H^{\mathrm{DPPC}} = 38.5$ kJ·mol^{-1} and $T_m^{\mathrm{DPPC}} = 41.8$°C for DPPC, obtained from our DSC experiments, and $\Delta H^{\mathrm{DOPC}} = 7.7$ kJ·mol^{-1} and $T_m^{\mathrm{DOPC}} = -21.3$°C obtained from literature. The mismatch energy of the interaction between neighboring lipids was set at $J = 0.31$. The theoretical model is in good agreement with our experimental data from Laurdan emission spectra and with the DOPC:DPPC phase diagram reported by Chen (35) (Fig. 5).

For systems containing styrene oligomers, we kept all model parameters constant, except for the different enthalpy and transition temperature obtained from calorimetry experiments, namely $\Delta H^{\mathrm{DPPC:SO}} = 30.7$ kJ·mol^{-1} and $T_m^{\mathrm{DPPC:SO}} = 41.5$°C, to calculate the new boundary line. The boundary line in presence of styrene oligomers indeed shows good agreement with our experimental observation (Fig. 5). This suggests that the thermodynamic changes induced by SO in DPPC bilayers is the main driving force behind depression of the liquidus line towards lower temperature.

Conclusions

Our results show that the incorporation of styrene oligomers in lipid bilayers is strongly coupled to membrane phase behaviour. In the low temperature gel phase, styrene short chains are laterally segregated in the membrane, as shown by SANS experiments. This segregation is due to the poor solubility of the oligomers in the tightly packed acyl chain region. Neutron scattering experiments also show that, as the bilayer melts from the gel to the L_α phase upon an increase of temperature, the oligomers become more uniformly distributed and intercalate between the acyl chains towards the water interface. This scenario is also supported by the strong variation of GP in the fluid phase, as well as by the close to linear dependence with polymer content of the Laurdan emission and of the transition enthalpy. Incorporation of the oligomers was also found to alter the gel-to-liquid main transition and the lipid packing of the membrane in the fluid phase, as shown by the Laurdan emission spectra. These changes can be ascribed to a preferential partition of the styrene chains into the fluid phase, thus depressing the gel-to-fluid transition temperature of the membrane. The evolution of the thermodynamic coexistence lines between pure bilayers and bilayers containing the short styrene chains is correlated with the change in enthalpy at the gel-fluid transition. In the case of the binary lipid system DOPC:DPPC the presence of the styrene oligomers shifts the S_o and L_α miscibility line towards lower temperatures: incorporated styrene oligomers have thus the potential to preclude domain formation. Our findings demonstrate that the presence of styrene chains in lipid bilayers affects the membranes phase behavior, and point to a likely disruption of biomembranes functionality by polymeric nanopollutants.

Materials and Methods

Materials. Chloroform solution of DOPC (1,2-dioleoyl-sn-glycero-3-phosphocholine, $C_{44}H_{84}NO_8P$, M_w 786.11), DPPC (1,2-dipalmitoyl-sn-glycero-3-phosphocholine, $C_{40}H_{80}NO_8P$, M_w = 734.039) were purchased from Avanti Polar Lipid (Birmingham, AL). DiI Stain (1,1'-Dioctadecyl-3,3,3',3'-Tetramethylindocarbocyanine Perchlorate $C_{59}H_{97}ClN_2O_4$, M_w = 933.8793) was provided by ThermoFisher Scientific (Waltham, MA, USA). Sucrose ($C_{12}H_{22}O_{11}$ M_w = 342.3) and Laurdan (6-Dodecanoyl-N,N-dimethyl-2-naphthylamine) were purchased from Sigma-Aldrich (Saint-Quentin, France). Atactic styrene oligomers ($(C_8H_8)_n$) M_n = 500 Da) was purchased from Polymer Source Inc. All chemicals had high purity and were used without further purification. The osmolarities of the sucrose solutions were measured with a cryoscopy osmometer Osmomat 030 (Gonotec; Berlin, Germany)

Multilamellar vesicles (MLVs) and large unilamellar vesicles (LUVs) preparation. For DSC experiments, MLVs were prepared by placing 1.5 mg of the desired lipid (with and without styrene oligomers) composition in chloroform in a glass vial, and organic solvent was evaporated using first an argon stream for 20 min, followed by 8 h of vacuum pumping. The lipid film was then hydrated with MilliQ distilled water (18.2 MΩ) at 70°C to reach the desired concentration and gently vortexed. The resulting MLV suspensions were sonicated for 15 min to disperse larger aggregates. In case of LAURDAN measurements, LUVs were prepared similarly to MLVs protocol with following modifications. The lipid solution in chloroform was mixed with 1% mol Laurdan in chloroform prior to evaporation. Upon swelling with MilliQ water and sonication, the MLVs solution was extruded using an Avanti Mini-Extruder 21 times through a 100 nm diameter pore polycarbonate filter.

Small unilamellar vesicles preparation. Liposome of the desired lipid composition were formed using either MilliQ distilled water (18.2 MΩ), H_2O/D_2O 92:8, or D_2O.For fluorescence measurements, the lipids were stained with 1% mol Laurdan in chloroform prior to evaporation. Liposomal solutions remained stable over a period of days. In case of liposomal suspension used in SANS experiments liposomes were then extruded using an Avanti Mini-Extruder. The sample was first extruded 21 times through 200 nm, subsequently 21 times through 100 nm and finally 21 times through 50 nm diameter pore polycarbonate filters.

Small Angle Neutron Scattering (SANS). The neutron wavelength resolution was $2 \cdot \Delta\lambda/\lambda = 0.1$. All scattering data were corrected for background, and incoherent scattering from 1 mm thick D_2O or H_2O solutions were used to correct for the deviation in uniformity of the detector response. The final data were converted to absolute scale. All experiments were first performed at low temperature (25 °C) and then at 50°C. SANS measurements for 100% D2O contrast were performed at 24.0, 8.0, 1.5 m detector distances at the D11 small angle instrument at ILL Grenoble, France. The wavelength of neutrons was set to 6 Å. The instrument was configured to provide an effective q-range of ∼0.01,Äì0.4 $Å^{-1}$. All SANS measurements were performed at 20°C and 50°C, well above the phase transition temperature of DPPC (∼42 °C). The SANS data from the position sensitive 2D detector was reduced to 1-D profiles I(q) vs. q, by using facility supplied data reduction software Lamp. Preliminary scattering data and measurements to determine the contrast matching conditions were obtained on the PACE spectrometer at the Laboratory Leon Brillouin (LLB) in Saclay, France.

Steady-state fluorescence. 3 mL of liposomal suspension stained with Laurdan of total concentration 3 mg/mL was placed in a quartz silica cuvette with 1 mm path length. Acquisition of Laurdan emission spectra was performed with a Jobin Horiba FluoroMax equipped with a Peltier unit to control temperature. Excitation wavelength was set at 350 nm with a bandpass of 1 nm and emission was also recorded with slit of 1 nm. The solution was equilibrated at given temperature for 10 min before each acquisition. For each sample (n=3) we performed two cycles of heating and cooling. General polarization (GP) was calculated using the standard expression provided by Parasassi (37). To quantify the miscibility temperature for each sample, we compared the GP plot from excitation 350 nm and 400 nm, and extrapolated the temperature range at which the two curves intersect. A full description of quantification is provided in the ESI.

Giant unilamellar vesicles preparation. GUVs composed of DOPC:DPPC, both in absence of presence of styrene oligomers, were prepared by electroformation following the protocol introduced by Angelova (38). Simply, 5 μl of 2 mg/mL solution of DOPC:DPPC or DOPC:DPPC:SO at the desired molar ratio, stained with 1% mol of DiI, in chloroform were spread on each cathode of a custom made electroformation stage. The stage was kept under vacuum for at least 1 hour to ensure complete evaporation of solvent and subsequently the lipid film was hydrated using sucrose solution (100 mosm/Kg) at 55°C. We applied a sinusoidal electric field of 1 V peak-peak intensity at 10 kHz for 1 hour while keeping the sample heated above the transition temperature. The resulting GUV suspension was kept at 20°C water bath to ensure complete stabilization of the sample. Vesicles were used on the same day of preparation.

Optical Microscopy and S_o phase-domain quantification. Imaging of GUVs labelled with 1% mol DiI was performed using a Nikon Eclipse TE2000-E microscope equipped with a Diagnostic Instruments NDIAG1800 camera and a Nikon 60x water immersion, NA 1.2 objective (Nikon). Observation was performed in the epifluorescence mode with a Hg lamp, 100 W (Intensilight, Nikon) as excitation source and adapted filtering TE/TRITC Ex 543/22 nm, DM 562 nm and Em 593/40 nm. GUVs samples were initially swelled by diluting the external medium with ∼5% volume of pure water. Prior to experimental observation, GUVs were kept at the desired temperature for at least 1 hour to stabilize. 100 μL of a GUVs solution were placed in a chamber. Quantification of S_o phase domains in vesicle was performed by measuring the radius of the domains, which was then corrected for by taking into account the spherical nature of the GUVs. A more detailed description of the quantification approach can be found in the SI. For each lipid composition we have quantified the domain area coverage from two separate samples, with 40 vesicles from each replicate.

Differential Scanning Calorimetry. The calorimetry measurements were performed with high sensitivity differential scanning calorimeter (μDSC Setaram). The measuring cell was filled with the sonicated sample, while the reference cell was filled with milliQ water. The temperature of the cells was changed with a constant rate (heating rate: 0.5 $K \cdot min^{-1}$, cooling rate: 0.3 $K \cdot min^{-1}$). The system was equilibrated ∼ 20 min before each heating or cooling ramp. The analysis of DSC data was performed using OriginPro 9.0 (Northampton, Ma, USA). For each sample (n=2) we performed three cycles of heating and cooling.

Dynamic light scattering (DLS). Liposomal suspension of lipid and lipid:SO vesicles were characterized by dynamic light scattering using Malvern Zetasizer Nano ZS. Simply, 1 mL of liposomal suspsension at 1 mg/mL was placed in a disposable plastic cuvette and light scattering recorded. Measurements were repeated at least 3 times for statistics.

ACKNOWLEDGMENTS. We thank Prof. Jian Liu (University of Manchester) and Prof. Olivier Sandre (University of Bordeaux) for providing their expertise in discussing the neutron scattering results. We also thank Annie Brûlet whom provided expertise and assisted in

the acquisition of the neutron scattering data at the Leon Brillouin Laboratory (LLB), and the Institute Laüe-Langevin in Grenoble and the LLB in Saclay for providing the facilities needed to conduct the neutron scattering experiment. The ISO9001 Characterization Platform of the Institut Charles Sadron is gratefully acknowledged for access to μDSC and fluorometer. M.I.M., M.K., F.T., A.P.S., and C.M.M. acknowledge funding from the European FP7-MSCA International Training Network SNAL 608184 (Smart Nano-Objects for Alteration of Lipid Bilayers) for support for this work.

1. M Haward, Plastic pollution of the world's seas and oceans as a contemporary challenge in ocean governance. *Nat. Commun.* **9** (2018).
2. SB Borrelle, et al., Opinion: Why we need an international agreement on marine plastic pollution. *Proc. Natl. Acad. Sci.* **114**, 9994–9997 (2017).
3. JR Jambeck, et al., Plastic waste inputs from land into the ocean. *Science* **347**, 768–771 (2015).
4. M Piccardo, M Renzi, A Terlizzi, Nanoplastics in the oceans: Theory, experimental evidence and real world. *Mar. Pollut. Bull.* **157**, 111317 (2020).
5. B Gewert, MM Plassmann, M MacLeod, Pathways for degradation of plastic polymers floating in the marine environment. *Environ. Sci.: Process. Impacts* **17**, 1513–1521 (2015).
6. M Cole, P Lindeque, C Halsband, TS Galloway, Microplastics as contaminants in the marine environment: A review. *Mar. Pollut. Bull.* **62**, 2588 – 2597 (2011).
7. MC Fossi, et al., Are baleen whales exposed to the threat of microplastics? a case study of the mediterranean fin whale (balaenoptera physalus). *Mar. Pollut. Bull.* **64**, 2374 – 2379 (2012).
8. A Collignon, et al., Neustonic microplastic and zooplankton in the north western mediterranean sea. *Mar. Pollut. Bull.* **64**, 861 – 864 (2012).
9. K Mattsson, LA Hansson, T Cedervall, Nano-plastics in the aquatic environment. *Environ. Sci.: Process. Impacts* **17**, 1712–1721 (2015).
10. Y Lu, Y Mei, R Walker, M Ballauff, M Drechsler, 'nano-tree'—type spherical polymer brush particles as templates for metallic nanoparticles. *Polymer* **47**, 4985 – 4995 (2006).
11. E Bergami, et al., Nano-sized polystyrene affects feeding, behavior and physiology of brine shrimp artemia franciscana larvae. *Ecotoxicol. Environ. Saf.* **123**, 18 – 25 (2016) 6th Biannual ECOtoxicology MEeting (BECOME 2014) - Environmental emergencies: ecotoxicology as a management tool.
12. MA Browne, A Dissanayake, TS Galloway, DM Lowe, RC Thompson, Ingested microscopic plastic translocates to the circulatory system of the mussel, mytilus edulis (l.). *Environ. Sci. & Technol.* **42**, 5026–5031 (2008).
13. M Al-Sid-Cheikh, et al., Uptake, whole-body distribution, and depuration of nanoplastics by the scallop pecten maximus at environmentally realistic concentrations. *Environ. Sci. & Technol.* **52**, 14480–14486 (2018).
14. K Saido, et al., New analytical method for the determination of styrene oligomers formed from polystyrene decomposition and its application at the coastlines of the north-west pacific ocean. *Sci. The Total. Environ.* **473-474**, 490 – 495 (2014).
15. G Rossi, J Barnoud, L Monticelli, Polystyrene nanoparticles perturb lipid membranes. *The J. Phys. Chem. Lett.* **5**, 241–246 (2014) PMID: 26276207.
16. D Bochicchio, E Panizon, L Monticelli, G Rossi, Interaction of hydrophobic polymers with model lipid bilayers. *Sci. Reports* **7**, 6357 (2017).
17. M Jung, et al., Interaction of styrene with dodab bilayer vesicles. influence on vesicle morphology and bilayer properties. *Langmuir* **16**, 968–979 (2000).
18. EZ Radlinska, et al., Polymer confinement in surfactant bilayers of a lyotropic lamellar phase. *Phys. Rev. Lett.* **74**, 4237–4240 (1995).
19. J Pencer, et al., Detection of submicron-sized raft-like domains in membranes by small-angle neutron scattering. *The Eur. Phys. J. E* **18**, 447–458 (2005).
20. TPT Dao, et al., Phase separation and nanodomain formation in hybrid polymer/lipid vesicles. *ACS Macro Lett.* **4**, 182–186 (2015).
21. LA Bagatolli, B Maggio, F Aguilar, CP Sotomayor, GD Fidelio, Laurdan properties in glycosphingolipid-phospholipid mixtures: a comparative fluorescence and calorimetric study. *Biochimica et Biophys. Acta (BBA) - Biomembr.* **1325**, 80 – 90 (1997).
22. SSW Leung, J Brewer, LA Bagatolli, JL Thewalt, Measuring molecular order for lipid membrane phase studies: Linear relationship between laurdan generalized polarization and deuterium nmr order parameter. *Biochimica et Biophys. Acta (BBA) - Biomembr.* **1861**, 183053 (2019).
23. QD Pham, D Topgaard, E Sparr, Cyclic and Linear Monoterpenes in Phospholipid Membranes: Phase Behavior, Bilayer Structure, and Molecular Dynamics. *Langmuir* **31**, 11067–11077 (2015).
24. AG Richter, et al., Scattering studies of hydrophobic monomers in liposomal bilayers: An expanding shell model of monomer distribution. *Langmuir* **27**, 3792–3797 (2011).
25. D Marsh, *Handbook of lipid bilayers, second edition.* (CRC Press), (2013).
26. A Rolland, A Brzokewicz, B Shroot, JC Jamoulle, Effect of penetration enhancers on the phase transition of multilamellar liposomes of dipalmitoylphosphatidylcholine. A study by differential scanning calorimetry. *Int. J. Pharm.* **76**, 217–224 (1991).
27. G Albertini, C Donati, R Phadke, M Ponzi Bossi, F Rustichelli, Thermodynamic and structural effects of propranolol on DPPC liposomes. *Chem. Phys. Lipids* **55**, 331–337 (1990).
28. AM Wolka, JH Rytting, BL Reed, BC Finnin, The interaction of the penetration enhancer DDAIP with a phospholipid model membrane. *Int. J. Pharm.* **271**, 5–10 (2004).
29. F Ollila, K Halling, P Vuorela, H Vuorela, J Slotte, Characterization of Flavonoid–Biomembrane Interactions. *Arch. Biochem. Biophys.* **399**, 103–108 (2002).
30. C Valenta, A Steininger, BG Auner, Phloretin and 6-ketocholestanol: Membrane interactions studied by a phospholipid/polydiacetylene colorimetric assay and differential scanning calorimetry. *Eur. J. Pharm. Biopharm.* **57**, 329–336 (2004).
31. S Borsacchi, et al., Phase transitions in hydrophobe/phospholipid mixtures: hints at connections between pheromones and anaesthetic activity. *Phys. Chem. Chem. Phys.* **18**, 15375–15383 (2016).
32. ML Schmidt, L Ziani, M Boudreau, JH Davis, Phase equilibria in dopc/dppc: Conversion from gel to subgel in two component mixtures. *The J. Chem. Phys.* **131**, 175103 (2009).
33. BR Lentz, Y Barenholz, TE Thompson, Fluorescence depolarization studies of phase transitions and fluidity in phospholipid bilayers. 2. two-component phosphatidylcholine liposomes. *Biochemistry* **15**, 4529–4537 (1976).
34. K Furuya, T Mitsui, Phase transitions in bilayer membranes of dioleoyl-phosphatidylcholine/dipalmitoyl-phosphatidylcholine. *J. Phys. Soc. Jpn.* **46**, 611–616 (1979).
35. D Chen, MM Santore, 1,2-dipalmitoyl-sn-glycero-3-phosphocholine (dppc)-rich domain formation in binary phospholipid vesicle membranes: Two-dimensional nucleation and growth. *Langmuir* **30**, 9484–9493 (2014).
36. J Wolff, CM Marques, F Thalmann, Thermodynamic approach to phase coexistence in ternary phospholipid-cholesterol mixtures. *Phys. Rev. Lett.* **106**, 128104 (2011).
37. T Parasassi, EK Krasnowska, L Bagatolli, E Gratton, Laurdan and Prodan as polarity-sensitive fluorescent membrane probes. *J. fluorescence* **8**, 365–373 (1998).
38. MI Angelova, DS Dimitrov, Liposome electroformation. *Faraday Discuss. Chem. Soc.* **81**, 303–311 (1986).